

Synthesis, spectroscopic characterization, X-ray crystal structure, antimicrobial, DNA-binding, alkaline phosphatase and insulin-mimetic studies of oxidovanadium(IV) complexes of azomethine precursors

Khurram Shahzad Munawar , Saqib Ali , Muhammad Nawaz Tahir , Nasir Khalid , Qamar Abbas , Irfan Zia Qureshi , Shabbir Hussain & Muhammad Ashfaq

To cite this article: Khurram Shahzad Munawar , Saqib Ali , Muhammad Nawaz Tahir , Nasir Khalid , Qamar Abbas , Irfan Zia Qureshi , Shabbir Hussain & Muhammad Ashfaq (2020): Synthesis, spectroscopic characterization, X-ray crystal structure, antimicrobial, DNA-binding, alkaline phosphatase and insulin-mimetic studies of oxidovanadium(IV) complexes of azomethine precursors, Journal of Coordination Chemistry, DOI: [10.1080/00958972.2020.1813282](https://doi.org/10.1080/00958972.2020.1813282)

To link to this article: <https://doi.org/10.1080/00958972.2020.1813282>

 View supplementary material [↗](#)

 Published online: 02 Sep 2020.

 Submit your article to this journal [↗](#)

 Article views: 4

 View related articles [↗](#)

 View Crossmark data [↗](#)



Synthesis, spectroscopic characterization, X-ray crystal structure, antimicrobial, DNA-binding, alkaline phosphatase and insulin-mimetic studies of oxidovanadium(IV) complexes of azomethine precursors

Khurram Shahzad Munawar^{a,b}, Saqib Ali^c, Muhammad Nawaz Tahir^d, Nasir Khalid^e, Qamar Abbas^f, Irfan Zia Qureshi^g, Shabbir Hussain^h and Muhammad Ashfaq^d

^aDepartment of Chemistry, University of Sargodha, Sargodha, Pakistan; ^bDepartment of Chemistry, University of Mianwali, Mianwali, Pakistan; ^cDepartment of Chemistry, Quaid-i-Azam University, Islamabad, Pakistan; ^dDepartment of Physics, University of Sargodha, Sargodha, Pakistan; ^eChemistry Division, Pakistan Institute of Nuclear Science & Technology, Islamabad, Pakistan; ^fDepartment of Physiology, University of Sindh, Jamshroo, Pakistan; ^gDepartment of Animal Sciences, Quaid-i-Azam University, Islamabad, Pakistan; ^hDepartment of Chemistry, Lahore Garrison University, Lahore, Pakistan

ABSTRACT

A series of novel azomethine precursors were synthesized by the condensation reactions of 3-(trifluoromethyl)benzenamine (tfmb) with 2-hydroxybenzaldehyde (HL¹) (tfmbs), 2,3-dihydroxybenzaldehyde (HL²) (tfmbdh), 2-hydroxy-1-naphthaldehyde (HL³) (tfmbnd) and 5-chloro-2-hydroxybenzaldehyde (HL⁴) (tfmbCl). The oxidovanadium(IV) complexes of the type [VO(tfmbs)₂] (1), [VO(tfmbdh)₂] (2), [VO(tfmbnd)₂] (3) and [VO(tfmbCl)₂] (4) were also prepared by the reaction of ligands HL¹–HL⁴ with vanadyl(V) isopropoxide [VO(OCHMe₂)₃]. The synthesized compounds were characterized by elemental analysis, FT-IR, multinuclear (¹H and ¹³C) NMR spectroscopies, magnetic susceptibility measurements and thermogravimetry. The studies revealed that binding of precursors with metal took place through azomethine nitrogen and phenolic oxygen. The single-crystal analysis of HL¹, HL⁴ and **3** has been carried out. The intercalation mode of interaction of the complexes with Salmon sperm DNA (SS-DNA) was established by the observed hypochromicity through UV–vis spectroscopic studies. The determined negative ΔG values confirmed the spontaneity of the binding process of complexes with SS-DNA. All the synthesized precursors and complexes were screened for their alkaline phosphatase inhibition, antimicrobial, hemolytic and insulin-mimetic properties, which exhibited significant activities with a few exceptions.

ARTICLE HISTORY

Received 25 February 2020
Accepted 21 July 2020

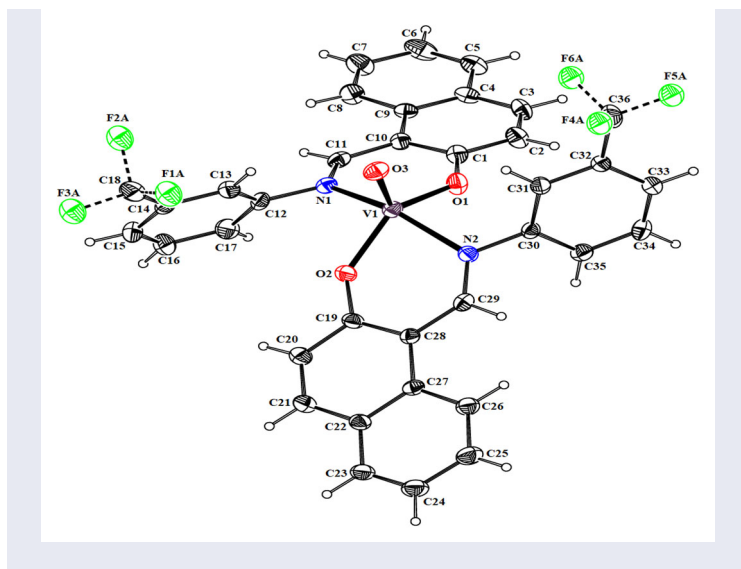
KEYWORDS

Oxidovanadium(IV) complexes; crystal structure; DNA-binding; insulin-mimetic studies; antimicrobial activity; alkaline phosphatase inhibition

CONTACT Khurram Shahzad Munawar  khurramchemist@gmail.com  Department of Chemistry, University of Sargodha, Sargodha, Pakistan; Saqib Ali  drsa54@hotmail.com  Department of Chemistry, Quaid-i-Azam University, Islamabad, Pakistan

 Supplemental data for this article is available online at <https://doi.org/10.1080/00958972.2020.1813282>.

© 2020 Informa UK Limited, trading as Taylor & Francis Group



1. Introduction

Recent advances in the coordination chemistry and catalytic properties of vanadium has attracted increasing interest during the last few years due to the model character of many of its complexes for the biological functions of vanadium [1–5], role of vanadium complexes in oxidation and oxo-transfer catalysis [6, 7] and potential medicinal application such as treatment of diabetes mellitus [8–10]. One likely mechanism for the insulin-mimetic activity of vanadium compounds is related to their potent inhibition of protein tyrosine phosphatases (PTPs) [11]. The reasons for the superior activity of vanadium compounds are not clear but could be related to better bioavailability of these compounds or more potent activity at the enzyme's active site.

Vanadium complexes have multiple biological and pharmacological activities, including antimicrobial [12], anti-leukemia [13], antitumor [14] and photodynamic therapy [15]. Vanadium complexes are further explored in DNA-binding and cleavage properties for their potential applications in the study of DNA structural probes and DNA-dependent electron-transfer mechanism [16–18]. The oxidative DNA-cleavage that involves the heterocyclic bases and/or sugar moiety finds application in footprinting and therapeutic studies [19]. Several Schiff bases of VO(IV) complexes, such as [VO(satsc)(phen)] (where satsc is salicylaldehyde thiosemicarbazone) [20], [VO(salmdtc)(B)] (where salmdtc is dianionic N-salicylidene-S-methylthiocarbamate and B is N,N-donor phenanthroline base) [21] have been synthesized and studied for their DNA-binding and cleavage activities. However, the mechanisms by which they interact with DNA have not yet been clearly elucidated [22].

Human alkaline phosphatase (ALP) can be classified into at least four tissue-specific forms or isozyme mainly according to the specificity of the tissue to be expressed, termed as placental alkaline phosphatase (PLALP or Regan isozyme), intestinal alkaline phosphatase (IALP), liver/bone/kidney alkaline phosphatase (L/B/K ALP) and germ cell ALP (GCALP or NAGAO isozyme).

ALP is important in recycling phosphate within living cells. It seems to be particularly prevalent in tissues which are transporting nutrients, including intestine and kidney. Inhibitors of ALP include vanadate, arsenate, L-phenylalanine and L-tryptophan. These inhibitors have been used in studies geared towards better understanding of the physiological role of ALP [23]. The rate of an enzyme-catalyzed reaction depends partly on how well the enzyme and substrate fit together. Thus, environmental factors (such as pH, temperature or presence of inhibitor) which might change the shape of either enzyme or substrate could alter the rate of formation of product. Vanadate in its monomeric form is a strong competitive inhibitor of wild-type ALP [24]. The inhibitory effect of vanadate has been ascribed to its mimetic ability to the anionic character of inorganic phosphate [25]. In fact, small-sized inorganic ions that include inorganic phosphate (~10 mM), vanadate (2 mM) and periodate (0.05 mM) [26, 27] are the most potent inhibitors of ALP.

Azomethine precursors are preferred over carboxylates and thiols in the present study because they have versatile applications and the most interesting is that they form the complex immediately just by stirring without the involvement of tedious reaction conditions. One problem found for carboxylate complexes is that we have to prepare its either sodium or potassium salt before complexation. Secondly, they have limited solubility. While the thiols makes S-S bridge during complexation which are sometime unavoidable. Another drawback is that, in some cases, SH at ortho-position makes a five-membered ring with carbon of aldehyde during the synthesis of ligands.

The substitution of phenolic group at ortho-position of the ligands is necessary from the coordination point of view that vanadium can chelate by using "O" of phenolic part and "N" of azomethine part to make a stable six-membered ring. The other substitutions in the ligands are to make the diversity and to elaborate the effect/change on the application/activity.

In the present work, azomethine precursors HL¹-HL⁴ and their oxidovanadium complexes **1-4** have been synthesized and characterized. The interactions of the synthesized compounds with Salmon sperm DNA (SS-DNA) were investigated using UV-vis absorption titration. All the compounds were checked for their inhibition against ALP. The synthesized compounds were tested for their *in vitro* antibacterial, antifungal and hemolytic activities. The insulin-enhancing properties were also elaborated by treating the diabetic mice with these compounds and then monitoring their blood plasma level.

2. Experimental

2.1. Materials

The reagents, vanadyl(V) isopropoxide, 3-(trifluoromethyl)benzenamine, 2-hydroxybenzaldehyde, 2,3-dihydroxybenzaldehyde, 2-hydroxy-1-naphthaldehyde, 5-chloro-2-hydroxybenzaldehyde, *p*-nitrophenyl phosphate hexahydrate (*p*-NPP), diethanolamine, Alloxan monohydrate and magnesium chloride were purchased from Sigma Aldrich (USA) and used without further purification. Sodium salt of SS-DNA was obtained from ACROS Organics and used as received. All the solvents like dimethylsulfoxide (DMSO), acetonitrile, ethanol, etc. were purchased from E. Merck (Germany). Human serum,

obtained from “Capital Development Authority” (CDA) hospital Islamabad, was used as a source of ALP.

All procedures performed in studies involving human participants were in accord with the ethical standards of the institutional and/or national research committee and with the 1964 Helsinki declaration and its later amendments or comparable ethical standards. All applicable institutional and/or national guidelines for the care and use of animals were followed.

2.2. Characterization of synthesized products

Elemental analysis of the synthesized compounds was carried out on an Elemental Vario EL elemental analyzer. FT-IR spectra in the range of 4000–400 cm^{-1} were obtained on a Thermo Nicolet-6700 FT-IR spectrophotometer. Multinuclear (^1H and ^{13}C) NMR spectra were recorded on a Bruker-400 MHz FT-NMR spectrometer using DMSO- d_6 as a solvent [δ ^1H (DMSO) = 2.5 ppm and δ ^{13}C (DMSO) = 39 ppm]. Chemical shifts are given in ppm and coupling constants (J) values are reported in Hz. The multiplicity of ^1H NMR signals (s = singlet, d = doublet, dd = doublets of doublet, t = triplet, dt = doublets of triplet and m = multiplet) are mentioned with chemical shifts. The absorption spectra were measured on a Shimadzu 1800 UV–visible spectrophotometer. The melting points were determined in capillary tubes using an electrothermal melting point apparatus (Gallenkamp). Magnetic moment was determined by using Sherwood magnetic susceptibility balance at ambient temperature ($25 \pm 2^\circ\text{C}$), using $\text{Hg}[\text{Co}(\text{SCN})_4]$ as calibrant. Thermogravimetric analysis was performed by Universal V4.3A TA Instruments. The XRD data of the titled compounds were collected using the diffractometer Bruker KAPPA Apex-II having monochromator made of graphite providing finely focused K_α X-rays, a CCD detector for recording of diffraction peaks. Apex-II (Bruker 2009), SHELXS97 and SHELXS2014/6 software were used for data collection, solution of structure and structure refinement, respectively. Thermal ellipsoid diagrams were drawn by ORTEP-3 software [28]. Packing of molecules for the compounds were shown by PLATON software whereas Mercury 4.0 was used for graphical representation of π – π stacking interaction.

2.3. SS-DNA binding studies by electronic absorption titration

SS-DNA (20 mg) was dissolved in doubly deionized water (pH = 7.0), kept at 4°C and used within 4 days. The SS-DNA solution gave a ratio of UV absorbance at 260 and 280 nm of 1.84:1, indicating that the DNA is sufficiently free from protein [29]. The DNA concentration was determined by measuring absorption intensity at 260 nm with the known molar absorption coefficient value of $6600 \text{ M}^{-1} \text{ cm}^{-1}$ [30] and was found to be $2.0 \times 10^{-4} \text{ M}$. The compound was dissolved in 70% DMSO:H₂O at a concentration of 2 mM. For UV absorption studies, 10 mL solution of SS-DNA and compound was prepared by varying the concentration of SS-DNA, while keeping the concentration of compound fixed, along with a reference solution without the compound. Compound–SS-DNA solutions were endorsed to incubate for 30 min at room temperature ($25 \pm 1^\circ\text{C}$) before the absorption measurements were made. The data were then

fitted into the following Benesi–Hildebrand equation to obtain the intrinsic binding constant, K [31]:

$$\frac{A_0}{A - A_0} = \frac{\varepsilon_G}{\varepsilon_{H-G} - \varepsilon_G} + \frac{\varepsilon_G}{\varepsilon_{H-G} - \varepsilon_G} \times \frac{1}{K[\text{DNA}]}$$

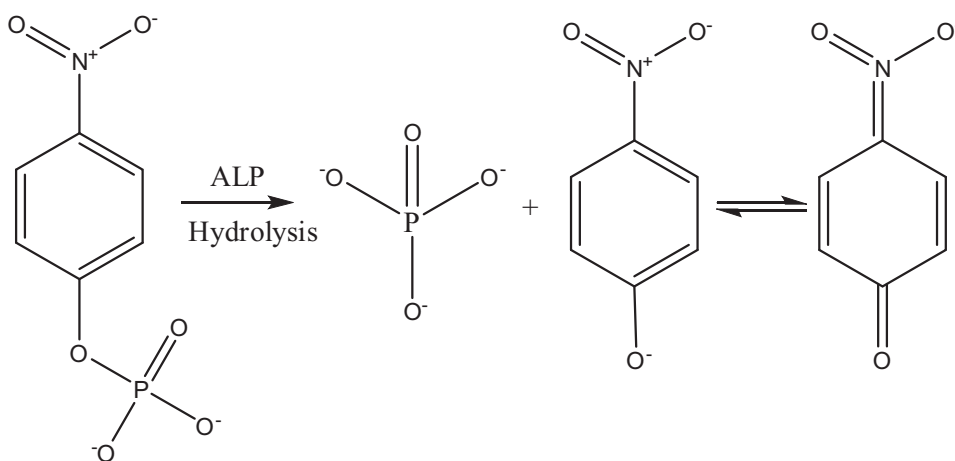
where K = binding constant, A_0 = absorbance of the compound, A = absorbance of the compound–SS-DNA adduct, ε_G = absorption coefficient of the compound and ε_{H-G} = absorption coefficient of the compound–SS-DNA adduct. The binding constants may be obtained from the intercept-to-slope ratios of $A_0/(A - A_0)$ versus $1/[\text{DNA}]$ plots. The change in Gibb's free energy (ΔG) may be determined using the following equation:

$$\Delta G = -RT \ln K$$

where R = general gas constant ($8.314 \text{ J K}^{-1} \text{ mol}^{-1}$), T = temperature (K) and K = binding constant.

2.4. ALP inhibition

For the preparation of assay, the method used was similar to the one as reported earlier with certain modifications [32]. Working substrate was made by mixing four parts of reagent A [diethanolamine (pH 9.8), 2 M and magnesium chloride 0.5 mM] and one part of reagent B [*p*-nitrophenyl phosphate (*p*-NPP) (50 mM)]. Substrate was incubated for 5 min at 25 °C. In a cuvette, 2 mL of the substrate was taken and 40 μL of human serum containing ALP having the activity of 165 IU L^{-1} was added. After incubation of 1 min, absorbance was measured to confirm the activity of enzyme which is termed as blank. ALP hydrolyzed the *p*-NPP and to give *p*-nitrophenol which produces yellow *p*-nitrophenolate ion under basic conditions according to the following reaction that absorbs at 405 nm.



For the purpose of inhibition studies of the synthesized compounds, the concentration of substrate and ALP was kept constant but the quantities of inhibitors, ligands, complexes and vanadium control (vanadyl(V) isopropoxide $[\text{VO}(\text{OCHMe}_2)_3]$) were

increased (10, 20, 30 and 40 μL) in each absorption studies periodically from 12.5 mM stock solution. Each sample was incubated for 3 min and the decrease in absorbance was recorded after every minute for at least 5 min. The average value of these was used to calculate the percentage inhibition. All ALP studies were carried out in triplicate.

2.5. Antimicrobial activities

The bacterial (*Escherichia coli*, *Bacillus subtilis*, *Staphylococcus aureus* and *Pasturella multocida*) and fungal (*Alternaria alternata*, *Ganoderma lucidum*, *Aspergillus niger* and *Penicillium notatum*) strains were cultured and inoculated by a reported procedure [33]. Antimicrobial potential of the ligands and their complexes was measured by disc diffusion method [34] with some modifications. Each filter paper disc (size, 9 mm) was soaked with 100 μL of a sample solution having concentration of 1 mg mL^{-1} of compound in DMSO and laid flat on growth medium. The petri plates were then incubated for 24 h at 37 $^{\circ}\text{C}$ for bacterial growth and 48 h at 28 $^{\circ}\text{C}$ for the growth of fungi. The biologically active samples form clear zones of inhibition around the discs which were measured in millimeters using a zone reader [33, 35].

2.6. Hemolytic activities

The hemolytic activities of azomethine precursors and their respective oxidovanadium complexes were carried out by an earlier reported procedure [33, 36]. The hemolysis percentage was calculated by the following formula [36]:

$$\% \text{ Hemolysis} = \frac{\text{Abs}_{(\text{sample})}}{\text{Abs}_{(\text{control})}} \times 100$$

2.7. Antidiabetic studies

2.7.1. Animals and maintenance

All animals were handled according to the guidelines provided by the local ethics committee of the "Department of Animal Sciences", on human use of animals for scientific research. Healthy adult male BALB/c mice ($n=50$, average body weight = 35 ± 5 g) were obtained from the National Institute of Health, Islamabad. Five animals were housed per cage and were given free access to standard rodent diet and water *ad libitum*. Photoperiod was maintained at 12:12 h light/dark cycle.

2.7.2. Induction of diabetes

Diabetes was induced by a single intraperitoneal injection (i.p.) of Alloxan monohydrate at the dose of 150 mg kg^{-1} body weight. Mice with fasting plasma glucose levels >200 mg dL^{-1} were considered diabetic and used for the current study.

2.7.3. Experimental design

Animals were divided into 10 groups, each containing five animals and treated with acute doses (35.9 mg kg^{-1} body weight) of $\text{HL}^1\text{-HL}^4$ and **1-4**. Positive control groups

were treated with a known antidiabetic drug Glibenclamide (Euglucon, Roche Pharma) in distilled water at the dose of 10 mg kg^{-1} body weight. Following were the treatment groups:

Control groups

Group 1: Negative control(diabetic, only Alloxan pretreated)

Group 2: Positive control(diabetic, Alloxan pretreated followed by Glibenclamide treatment)

Experimental groups

Animals of this group were diabetic, Alloxan pretreated. Groups 3–6 were treated with ligands HL¹–HL⁴, while Groups 7–10 were treated with complexes 1–4.

2.7.4. Determination of plasma glucose concentration

Blood was collected through caudal venipuncture using a 26 gauge butterfly cannula. Blood samples were drawn at 0 h (Pre-Alloxan), 1 h (Post-Alloxan) and then at 1, 2, 3, 4, 5, 6 and 7 h after dosing with the respective compounds. Plasma glucose levels were determined with a dextrostix using glucometer (Accu-Check Active, Roche).

2.7.5. Determination of total serum cholesterol and triglycerides

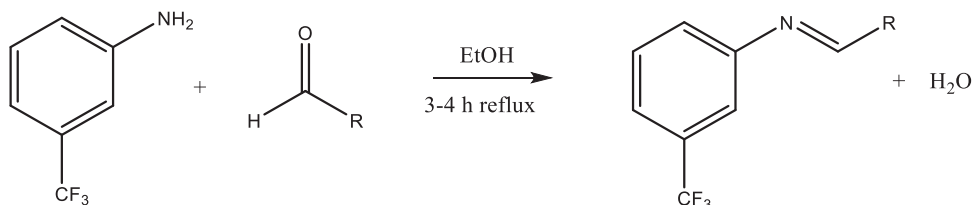
Total serum cholesterol and triglyceride concentrations were determined with commercially available kits obtained from Globe Diagnostics S.r.l (Italy) using Microlab 300 (Germany).

2.7.6. Statistical analysis

Data were analyzed through one-way analysis of variance (ANOVA) using the Statistical Package for Social Sciences (SPSS version 16.0 Inc., Chicago, Illinois, USA) Post-hoc Tukey-Kramer test. Where normality test failed, ANOVA on ranks was applied. $p < .05$ was considered statistically significant difference. Data are presented as line or bar diagrams constructed using the Graph Pad Prism 5 (Version 5.01 Graph Pad Software Inc., USA).

2.8. Syntheses of azomethine precursors

The general method for the synthesis of azomethine precursors is shown in the following generalized equation:



where "R" is 2-hydroxyphenyl (HL¹), 2,3-dihydroxyphenyl (HL²), 2-hydroxynaphthyl (HL³), 5-chloro-2-hydroxyphenyl (HL⁴).

2.8.1. Synthesis of (E)-2-((3-(trifluoromethyl)phenylimino)methyl)phenol (HL¹)

Stoichiometric amounts of 3-(trifluoromethyl)benzenamine and 2-hydroxybenzaldehyde (5 mmol of each) were added to 100 mL of dried ethanol. The mixture was refluxed for 3–4 h. The volume of reaction mixture was reduced to one-third of its original and left for crystallization at room temperature. Light yellow crystals were obtained after 2–3 days. Yield: 69%; m.p.: 85 °C; IR (ν/cm^{-1}): 3445 (–OH), 1609 (HC=N), 1109 (C–F); ¹H NMR (DMSO-d₆, 400 MHz), δ (ppm): 12.86 (s, –OH), 8.66 (s, HC=N), 7.54–7.58 (m), 7.41–7.50 (m), 7.07 (dd, J [¹H–¹H] = 5.7, 1.2 Hz), 6.70 (dt, J [¹H–¹H] = 7.5, 1.2 Hz); ¹³C NMR (DMSO-d₆, 101 MHz), δ (ppm): 149.2, 119.3, 123.4 (q, C–CF₃, ² J [¹⁹F–¹³C] = 3.75 Hz), 130.0, 132.1, 131.7, 118.0 (q, CF₃, ¹ J [¹⁹F–¹³C] = 3.75 Hz), 164.2 (HC=N), 118.9, 161.1 (C–OH), 117.4, 133.8, 124.6, 132.1.

2.8.2. Synthesis of (E)-3-((3-(trifluoromethyl)phenylimino)methyl)benzene-1,2-diol (HL²)

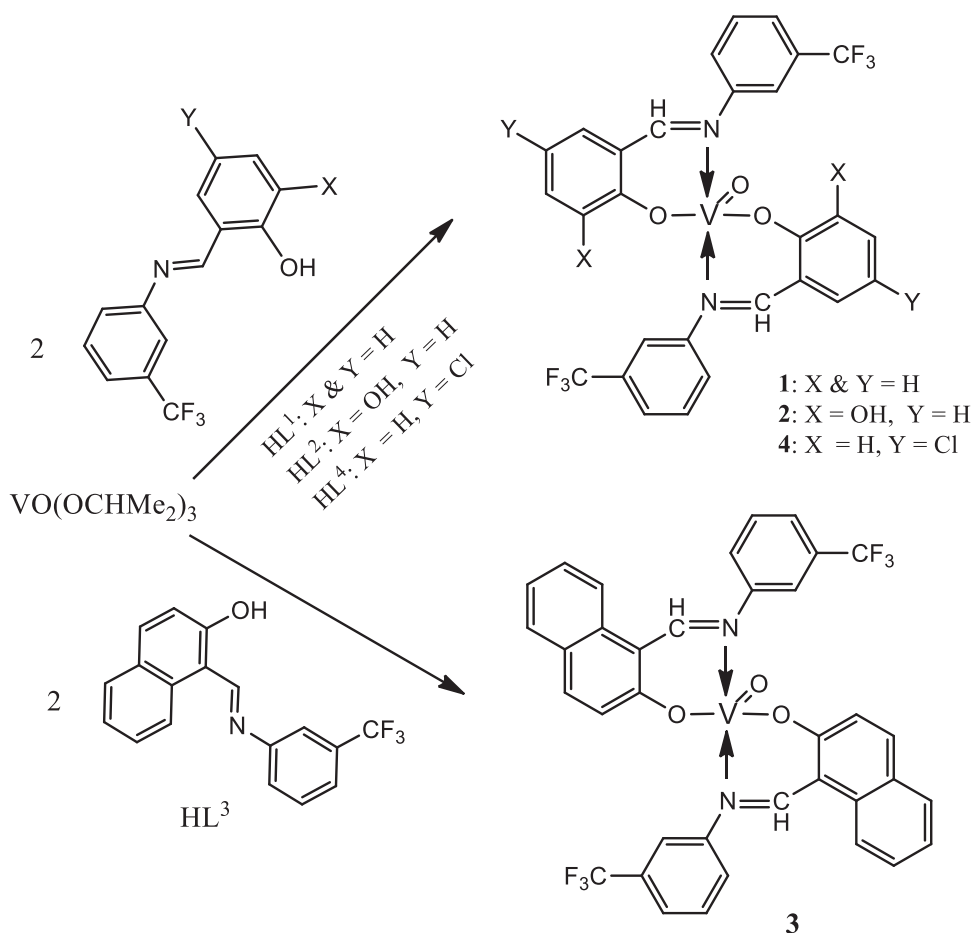
Similar procedure was adopted as described for HL¹, but instead of using 2-hydroxybenzaldehyde, 2,3-dihydroxybenzaldehyde was used. Yellow crystals were collected from the mother liquor after 24 h. Yield: 85%; m.p.: 116 °C; IR (ν/cm^{-1}): 3454 (–OH), 1616 (HC=N), 1106 (C–F); ¹H NMR (DMSO-d₆, 400 MHz), δ (ppm): 12.66 (s, –OH), 9.29 (s, –OH'), 9.00 (s, HC=N), 7.79 (s), 7.72–7.66 (m), 6.98 (dd, J [¹H–¹H] = 8.0, 1.2 Hz), 6.81 (t, J [¹H–¹H] = 8.0 Hz), 7.24 (dd, J [¹H–¹H] = 8.0, 1.2 Hz); ¹³C NMR (DMSO-d₆, 101 MHz), δ (ppm): 149.6, 119.4, 135.6 (q, C–CF₃, ² J [¹⁹F–¹³C] = 3.75 Hz), 123.5, 131.1, 126.2, 125.8 (q, CF₃, ¹ J [¹⁹F–¹³C] = 3.75 Hz), 166.2 (HC=N), 118.4, 149.5 (C–OH), 146.0 (C–OH'), 117.5, 119.8, 123.4.

2.8.3. Synthesis of (E)-1-((3-(trifluoromethyl)phenylimino)methyl)naphthalen-2-ol (HL³)

For the preparation of HL³, same procedure was adopted as described for HL¹, but instead of using 2-hydroxybenzaldehyde, 2-hydroxy-1-naphthaldehyde was used. Yellow crystals were collected from the mother liquor after one day. Yield: 84%; m.p.: 144 °C; IR (ν/cm^{-1}): 3449 (–OH), 1621 (HC=N), 1115 (C–F); ¹H NMR (DMSO-d₆, 400 MHz), δ (ppm): 12.10 (s, –OH), 9.76 (s, HC=N), 8.07 (s), 7.83 (dd, J [¹H–¹H] = 8, 1.2 Hz), 7.72 (t, J [¹H–¹H] = 8.0 Hz), 7.65 (d, J [¹H–¹H] = 8.0 Hz), 7.07 (d, J [¹H–¹H] = 9.2 Hz), 7.98 (d, J [¹H–¹H] = 9.2 Hz), 8.57 (dd, J [¹H–¹H] = 8.0, 1.2 Hz), 7.39 (d, J [¹H–¹H] = 8.0, 1.2 Hz), 7.58 (dt, J [¹H–¹H] = 8.0, 1.2 Hz), 7.90 (dd, J [¹H–¹H] = 8, 1.2 Hz); ¹³C NMR (DMSO-d₆, 101 MHz), δ (ppm): 146.1, 117.8, 117.7 (q, C–CF₃, ² J [¹⁹F–¹³C] = 3.75 Hz), 121.1, 127.3, 123.0, 123.1 (q, CF₃, ¹ J [¹⁹F–¹³C] = 3.75 Hz), 169.4 (HC=N), 109.3, 158.3 (C–OH), 117.7, 133.4, 127.3, 125.6, 121.2, 124.1, 121.1, 137.5.

2.8.4. Synthesis of (E)-4-chloro-2-((3-(trifluoromethyl)phenylimino)methyl)phenol (HL⁴)

Procedure adopted for the preparation of HL⁴ was similar as described for HL¹, but instead of using 2-hydroxybenzaldehyde, 5-chloro-2-hydroxybenzaldehyde was used. Yellow crystals were collected from the mother liquor within 24 h. Yield: 84%; m.p.: 88 °C; IR (ν/cm^{-1}): 3452 (–OH), 1615 (HC=N), 1109 (C–F); ¹H NMR (DMSO-d₆, 400 MHz), δ (ppm): 12.50 (s, –OH), 8.99 (s, HC=N), 7.78–7.79 (m), 7.68–7.71 (m), 7.03



Scheme 1. Synthesis of oxidovanadium complexes 1–4.

(d, J [^1H – ^1H] = 8.8 Hz), 7.45 (dd, J [^1H – ^1H] = 8.8, 2.8 Hz); ^{13}C NMR (DMSO- d_6 , 101 MHz), δ (ppm): 148.7, 123.7, 123.8 (q, C– CF_3 , 1J [^{19}F – ^{13}C] = 3.75 Hz), 134.5, 131.8, 130.1, 118.2 (q, CF_3 , 1J [^{19}F – ^{13}C] = 3.75 Hz), 162.9 (HC = N), 119.6, 159.7 (C–OH), 119.0, 133.6, 131.5 (C–Cl), 132.3.

2.8.5. Syntheses of $[\text{VO}(\text{tfmbs})_2]$ (1), $[\text{VO}(\text{tfmbdh})_2]$ (2), $[\text{VO}(\text{tfmbnd})_2]$ (3) and $[\text{VO}(\text{tfmbCl})_2]$ (4)

Oxidovanadium complexes **1–4** were synthesized by dropwise mixing of $\text{VO}(\text{OCHMe}_2)_3$ with ligands in 1:2 ratio using acetonitrile as a solvent (Scheme 1). The green products of **1**, **2** and **4** were precipitated out immediately, which were washed with acetonitrile and then air dried. However, **3** was obtained by refluxing the mixture for 1 h. On cooling, needle-shaped dark green crystals settled at the bottom. These crystals were filtered, washed with acetonitrile and air dried.

Complex **1**: Yield: 83%; m.p.: $>300^\circ\text{C}$; IR (ν/cm^{-1}): 1595 (HC = N), 1118 (C–F), 969 (V = O), 599 (V–O); Anal. Calcd for $[\text{C}_{28}\text{H}_{18}\text{F}_6\text{N}_2\text{O}_3\text{V}]$ (MW = 595.4) (%): C, 56.48; H, 3.05; N, 4.71; O, 8.06. Found: C, 56.32; H, 2.83; N, 4.82; O, 8.21. $\mu_{\text{eff}} = 1.84$ BM.

Complex **2**: Yield: 84%; m.p.: $>300^{\circ}\text{C}$; IR (ν/cm^{-1}): 1601 (HC=N), 1119 (C-F), 975 (V=O), 540 (V-O); Anal. Calcd for $[\text{C}_{28}\text{H}_{18}\text{F}_6\text{N}_2\text{O}_5\text{V}]$ (MW = 627.4) (%): C, 53.60; H, 2.89; N, 4.47; O, 12.75. Found: C, 53.84; H, 2.75; N, 4.52; O, 12.84. $\mu_{\text{eff}} = 2.17$ BM.

Complex **3**: Yield: 88%; m.p.: $>300^{\circ}\text{C}$; IR (ν/cm^{-1}): 1620 (HC=N), 1119 (C-F), 967 (V=O), 563 (V-O); Anal. Calcd for $[\text{C}_{36}\text{H}_{22}\text{F}_6\text{N}_2\text{O}_3\text{V}]$ (MW = 695.4) (%): C, 62.17; H, 3.19; N, 4.03; O, 6.90. Found: C, 62.35; H, 3.11; N, 4.23; O, 6.70. $\mu_{\text{eff}} = 2.10$ BM.

Complex **4**: Yield: 82%; m.p.: $>300^{\circ}\text{C}$; IR (ν/cm^{-1}): 1605 (HC=N), 1118 (C-F), 969 (V=O), 565 (V-O); Anal. Calcd for $[\text{C}_{28}\text{H}_{16}\text{F}_6\text{N}_2\text{O}_3\text{V}]$ (MW = 664.3) (%): C, 50.63; H, 2.43; N, 4.22; O, 7.23. Found: C, 50.73; H, 2.35; N, 4.32; O, 7.15. $\mu_{\text{eff}} = 2.17$ BM.

3. Results and discussion

The synthesis, spectroscopic and analytical data of prepared azomethine precursors and their respective oxidovanadium complexes are presented in Section 2. All the synthesized ligands HL¹–HL⁴ and their complexes **1**–**4** are in solid state, stable at room temperature. Ligands are soluble in organic solvents like DMSO, ethanol and chloroform, but complexes are only soluble in DMSO. The ligands and complexes were characterized by elemental analysis, FT-IR, multinuclear (¹H and ¹³C) NMR studies, single-crystal X-ray crystallography and thermogravimetric analysis.

3.1. FT-IR studies

The FT-IR spectra of free HL¹–HL⁴ showed bands of medium intensity in the range of 1609–1621 cm^{-1} due to azomethine $\nu(\text{HC}=\text{N})$ stretching. Coordination of the azomethine nitrogen with vanadium atom was expected to give a shift of $\nu(\text{HC}=\text{N})$ to lower wavenumber (1595–1605 cm^{-1}) as mentioned in Section 2; this effect is in fact observed for **1**, **2** and **4** while for **3** the $\nu(\text{HC}=\text{N})$ was not shifted at all which could probably be due to extra stability gained by the influence of the conjugated aromatic ring system attached to the azomethine moiety. This observed shifting of $\nu(\text{HC}=\text{N})$ stretching band in complexes suggests the coordination of the azomethine nitrogen to vanadium. The phenolic oxygen $\nu(-\text{OH})$ band appeared in the range of 3445–3454 cm^{-1} for free Schiff base ligand was disappeared upon complexation, due to the formation of the $\nu(\text{V}-\text{O})_{\text{phenolic}}$ [37]. The metal-terminal oxygen stretching $\nu(\text{V}=\text{O})$ in the complexes appeared as a single sharp peak in the range of 967–975 cm^{-1} , indicating that the oxidovanadium(IV) complexes have no intermolecular interaction with other oxidovanadium moiety [38]. The appearance of new bands in all FT-IR spectra of complexes in the range of 565–599 cm^{-1} could be attributed to the V–O bonds formed during the complexation. Thus, based on the infrared data, it is concluded that the azomethine precursors behave as monobasic bidentate, coordinating through azomethine N and phenolic O atoms.

3.2. NMR spectroscopy

Deuterated dimethylsulfoxide (DMSO- d_6) was used to record the ¹H and ¹³C NMR spectra of the ligands. The detailed chemical shifts of the diverse kinds of protons and

carbons have been reported in Section 2. The synthesis of HL¹–HL⁴ was confirmed by the appearance of peaks due to azomethine protons (HC=N) in the range of 8.66–9.76 ppm. The hydrogen bonded phenolic proton (–OH) gave downfield signals from 12.10 to 12.86 ppm whereas the second phenolic proton (–OH') in HL² has a slightly upfield signal at 9.29 ppm. Aromatic protons gave signals in the range of 6.70–7.83 ppm. ¹³C NMR spectra further support the formation of HL¹–HL⁴ by the signals of azomethine carbon (HC=N) in the range of 162.9–169.4 ppm. Fluorine showed coupling with the neighboring carbons by giving two quartets with the same coupling constant of 3.75 Hz surprisingly. ¹H NMR spectra of HL² and HL⁴ are shown in Figures S1 and S2.

3.3. Crystal structures of HL¹, HL⁴ and **3**

Crystal data and structure refinements of HL¹, HL⁴ and **3** are reported in Table 1 whereas details of hydrogen bonding and geometrical parameters (Å) for π – π stacking for **3** are listed in Tables 2 and 3. Figures 1–4 show the molecular structures along with atomic numbering schemes. The observed bond lengths and angles in all the ligand precursors are similar to the reported values for similar compounds [39].

In HL¹ (Figure 1, Table 1), the *o*-cresol moiety A (C1–C7/O1) and *m*-toluidine moiety B (C8–C14/N1) is planar with r.m.s. deviation of 0.0344 and 0.0119 Å, respectively. The dihedral angle A/B is 41.1(7)°. In (trifluoromethyl)benzene, the fluorine atoms are disordered over three sets of sites with occupancy ratio 0.364(3):0.335(3):0.301(3). The dihedral angles between major part of disordered fluorine moiety C (F1A–F3A), the intermediate disordered fluorine moiety D (F1B–F3B) and the minor part of disordered fluorine moiety E (F1C–F3C) C/D, D/E and C/E is 13.01(1)°, 4.97(2)° and 18.03(7)°, respectively. The dihedral angles B/C and B/D are 78.16(4)°, 88.97(37)° and 84.08(49)°, respectively; these dihedral angles show that the *m*-toluidine moiety B is nearly perpendicular to the disordered fluorine moieties D and E, respectively. The crystal exists in tautomeric form, as the phenolic hydrogen is not transferred to nitrogen of amine. Intramolecular hydrogen bonding exists, since the OH group of *o*-cresol moiety A interacts with nitrogen of *m*-toluidine moiety B through O–H...N bonding to form S(6) loop [40] (as shown in Figure S3 and given in Table 2). No intermolecular hydrogen bonding found in the crystal packing.

In HL⁴ (Figure 2, Table 1), the 4-chloro-2-methylphenol moiety A (C1–C7/O1/CL1) and *m*-toluidine moiety B (C8–C14/N1) is planar with r.m.s. deviation of 0.0110 and 0.0174 Å, respectively. The dihedral angle A/B is 7.62(2)°, indicating that moieties A and B are nearly parallel to each other. In (trifluoromethyl)benzene, the fluorine atoms are disordered over three sets of sites with occupancy ratio 0.436(3):0.315(3):0.249(3). The dihedral angles between the part-I of disordered fluorine moiety C (F1A–F3A), part-II of disordered fluorine moiety D (F1B–F3B) and part-III of disordered fluorine moiety E (F1C–F3C) C/D, D/E, E/C are 13.02(8)°, 5.38(1)° and 13.46(9)°, respectively. The dihedral angles B/C, B/D and B/E are 84.48(37)°, 83.56(49)° and 86.28(52)°, respectively; these dihedral angles show that the *m*-toluidine moiety B is nearly perpendicular to the disordered fluorine moieties C, D and E, respectively. Strong intramolecular O–H...N hydrogen bonding exists between the OH group of *o*-cresol moiety A and the nitrogen atom

Table 1. Crystallographic data of HL¹, HL⁴ and **3**.

Crystal data	HL ¹	HL ⁴	3
CCDC	983946	1986011	983950
Chemical formula	C ₁₄ H ₁₀ F ₃ NO	C ₁₄ H ₉ ClF ₃ NO	C ₃₆ H ₂₂ F ₆ N ₂ O ₃ V
<i>M_r</i>	265.23	299.68	695.49
Crystal system, space group	Monoclinic, P ₂ /c	Monoclinic, P 21/n	Orthorhombic, P 21 21 21
Temperature (K)	296	296	296
<i>a</i> , <i>b</i> , <i>c</i> (Å)	13.894(3), 11.509(2), 7.7124(10)	4.6497(5), 20.399(4), 13.792(3)	11.6947(10), 4.7795(13), 17.8542(13)
α , β , γ (°)	90, 101.590(2), 90	90, 94.633(4), 90	90, 90, 90
<i>V</i> (Å ³)	1208.1(3)	1303.9(4)	3086.0(4)
<i>Z</i>	4	4	4
Density (calculated) (mg/m ³)	1.458	1.771	1.497
<i>F</i> (0 0 0)	544	708	1412
Radiation type	Mo <i>K</i> α	Mo <i>K</i> α	Mo <i>K</i> α
Wavelength (λ) (Å)	0.71073	0.71073	0.71073
μ (mm ⁻¹)	0.12	0.711	0.398
Crystal size (mm)	0.38 × 0.16 × 0.14	0.40 × 0.20 × 0.16	0.34 × 0.20 × 0.18
<i>Data collection</i>			
Diffractometer	Bruker APEXII CCD diffractometer	Bruker APEXII CCD diffractometer	Bruker APEXII CCD diffractometer
Absorption correction	Absorption correction: multi-scan (SADABS; Bruker, 2007)	Absorption correction: multi-scan (SADABS; Bruker, 2007)	Absorption correction: multi-scan (SADABS; Bruker, 2007)
No. of measured, independent and observed [<i>I</i> > 2 <i>s</i> (<i>I</i>)] reflections	9246, 2369, 1007	7995, 2563, 1233	25367, 6711, 3475
<i>R</i> _{int}	0.070	0.0607	0.0780
Theta range for data collection (°)	1.496–25.997	2.486–25.999	1.789–26.997
Index ranges	−17 ≤ <i>h</i> ≤ 17, −14 ≤ <i>k</i> ≤ 14, −9 ≤ <i>l</i> ≤ 9	−5 ≤ <i>h</i> ≤ 5, −24 ≤ <i>k</i> ≤ 25, −16 ≤ <i>l</i> ≤ 16	−14 ≤ <i>h</i> ≤ 14, −18 ≤ <i>k</i> ≤ 18, −22 ≤ <i>l</i> ≤ 19
(<i>sin</i> θ / λ) _{max} (Å ⁻¹)	0.617	0.611	0.639
<i>Refinement</i>			
<i>R</i> [<i>F</i> ² > 2 σ (<i>F</i> ²)], <i>wR</i> (<i>F</i> ²), <i>S</i>	0.059, 0.190, 0.98	0.0732, 0.2052, 1.024	0.0593, 0.1287, 0.987
No. of reflections	2369	2563	6711
No. of parameters	197	203	448
No. of restraints	19	19	247
H-atom treatment	H atoms treated by a mixture of independent and constrained refinement	H-atom parameters constrained	H-atom parameters constrained
$\Delta\rho_{\max}$, $\Delta\rho_{\min}$ (e Å ⁻³)	0.24, −0.29	0.32, −0.35	0.27, −0.31

of *m*-toluidine moiety B through N–H ··· O bonding to form S(6) loop. The molecules are connected with each other in the form of dimers through C–H ··· F bonding to complete R₁²(4) loop. These loops are shown in Figure S4 and given in Table 2.

In **3** (Figure 3, Table 1), the coordination sphere around the vanadium atom consists of three oxygen atoms and two nitrogen atoms. Both ligands are chelating the central vanadium atom in *trans*-configuration with respect to each other. The vanadyl oxygen is at distance of 1.597(5) Å while the chelating oxygen atoms (O1/O3) are at the distance of 1.8969(40) and 1.9080(41) Å, respectively, from central vanadium atom. The chelating nitrogen atoms (N1/N2) are at the distances of 2.0904(49) and 2.0935(50) Å, respectively, from central vanadium atom, the equatorial bond angles range from 114.6(2)° to 130.7(2)° while the axial angles range from 84.2(2)° to 102.5(2)°, thus forming a distorted

Table 2. Hydrogen-bond geometry (Å, °) of HL¹, HL⁴ and **3**.

Compounds	D—H...A	D—H	H...A	D...A	D—H...A
HL ¹	O1—H1...N1	0.83(1)	1.85(2)	2.625(3)	155(4)
HL ⁴	O(1)—H(1)...N(1)	0.82	1.88	2.605(5)	146.9
	C(9)—H(4)...F(2B) ⁱ	0.93	2.50	3.339(14)	150.0
	C(9)—H(4)...F(2C) ⁱ	0.93	2.53	3.454(14)	173.3
3	C(2)—H(2)...F(3B) ⁱⁱ	0.93	2.56	3.298(13)	136.8
	C(35)—H(35)...F(5A) ⁱⁱⁱ	0.93	2.54	3.277(13)	136.9
	C(35)—H(35)...F(4B) ⁱⁱⁱ	0.93	2.57	3.137(13)	119.8
	C—H...Cg	C—H	H...Cg	C...Cg	C—H...Cg
	C34—H34...Cg3 ⁱⁱⁱ	0.93	2.84	3.383(8)	119

Symmetry transformations used to generate equivalent atoms: (i) $-x, -y + 1, -z$; (ii) $-x + 1/2, -y, z - 1/2$, (iii) $x + 1/2, -y + 1/2, -z$, where Cg3 is the centroid of one of the benzene rings of naphthalene (C1–C10) directly attached to O-atom of (Z)-3-iminoprop-1-en-1-ol moiety A.

Table 3. Geometrical parameters (Å) for π - π stacking for **3**.

Ring i–j ^a	R _c ^b	R1v ^c	R2v ^d	α ^e	β ^f	γ ^g	Slippage
Cg3...Cg6 ^{iv}	3.474(4)	−3.3536(13)	−3.454(3)	2.2(3)	6.2	5.3	–
Cg1...Cg7 ^{iv}	3.989(3)	−3.497(2)	−3.570(3)	2.3(3)	26.5	28.8	–
Cg5...Cg6 ^v	4.011(4)	3.995(3)	−3.702(3)	26.0(3)	22.6	5.1	–
Cg7...Cg3 ^{vi}	4.124(4)	−3.515(3)	−3.481(3)	0.9(3)	32.4	31.5	–
Cg4...Cg2 ^{vi}	4.174(4)	−3.580(3)	−3.383(2)	5.8(3)	35.8	30.9	–
Cg2...Cg3 ^{vi}	4.187(3)	−3.351(2)	−3.554(3)	6.7(3)	31.9	36.8	–
Cg1...Cg6 ^{iv}	4.285(3)	−3.534(2)	−3.521(3)	2.3(3)	34.7	34.4	–

Symmetry codes: (iv) $1/2 - x, -y, -1/2 + z$, (v) $1 - x, -1/2 + y, 1/2 - z$, (vi) $1/2 - x, -y, 1/2 + z$.

^aCg1, Cg2, Cg3, Cg4, Cg5, Cg6, Cg7 and Cg8 are the centroids of (C1/C10/C11/N1/O1/V1), (C19/C28/C29/N2/O2/V1), (C1–C4/C9/C10), (C4–C9), (C12 C17), (C19–C22/C27/C28), (C22–C27) and (C30–C35) rings.

^bCentroid–centroid distance between rings i and j.

^cVertical distance from ring centroid i to ring j.

^dVertical distance from ring centroid j to ring i.

^eDihedral angle between the first ring mean plane and the second ring mean plane of the partner molecule.

^fAngle between the centroid of the first ring and the second ring.

^gAngle between the centroid of the first ring and the normal to the mean plane of the second ring of the partner molecule.

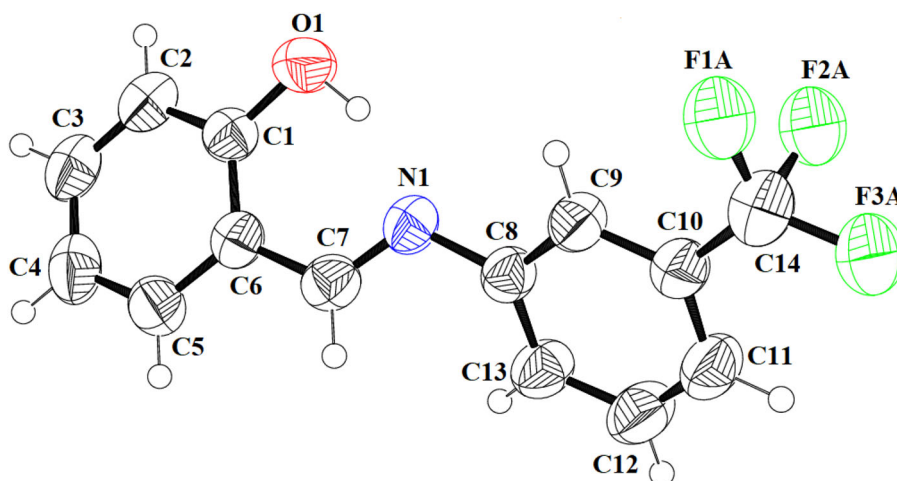


Figure 1. ORTEP diagram of (E)-2-(((3-(trifluoromethyl)phenyl)imino)methyl)phenol (HL¹) drawn at 50% probability level. The minor part of disordered trifluoro moiety is not shown for clarity and the hydrogens are shown by small circles of arbitrary radii.

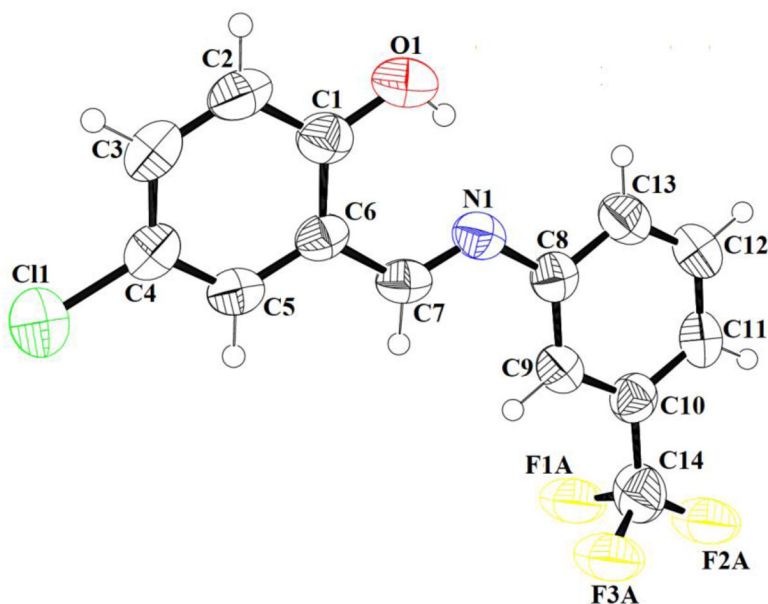


Figure 2. ORTEP diagram of (E)-4-chloro-2-((3-(trifluoromethyl)phenyl)imino)methyl)phenol (HL⁴) drawn at 50% probability level. The minor parts of disordered trifluoro moiety are not shown for clarity and the hydrogens are shown by small circles of arbitrary radii.

square pyramidal geometry with the τ value of 0.42 [41]. In both chelating ligands, the trifluoro moiety is disordered over three sets of sites with occupancy ratio of 0.444(8):0.341(8):0.215(5) with all disordered atoms set at equal anisotropic displacement parameters during refinement of structure. In the first chelating ligand (C1–C18/N1/O1/F1–F3), the (*Z*)-3-iminoprop-1-en-1-ol moiety A (C1/C10/C11/N1/O1), the naphthalene moiety B (C1–C10) and benzyl moiety C (C12–C18) are planar with r.m.s. deviation of 0.0224, 0.0142 and 0.0064 Å, respectively. The dihedral angles A/B and C/A are 0.62(3)° and 57.7(2)°, respectively. The dihedral angle between the (*Z*)-3-iminoprop-1-en-1-ol moiety A and the naphthalene moiety B indicates that these moieties are almost parallel to each other. In the second chelating ligand (C19–C36/N2/O2/F4–F6), the (*Z*)-3-iminoprop-1-en-1-ol moiety D (C19/C28/C29/N2/O2), the naphthalene moiety E (C19–C28) and benzyl moiety F (C30–C36) are planar with r.m.s. deviation of 0.0175, 0.0142 and 0.0103 Å, respectively. The dihedral angles D/E and F/D are 2.02(3)° and 66.02(2)°, respectively. The dihedral angle between the (*Z*)-3-iminoprop-1-en-1-ol moiety A and the naphthalene moiety B indicates that these moieties are almost parallel to each other. The molecules are connected with each other through C–H...F bonding (Figure S5 and Table 2). Another type of non-covalent interaction known as π – π stacking interaction exists with centroid–centroid distances ranges from 3.474(4) to 5.946(4) Å which helps in further stabilization of crystal packing [42]. The strongest π – π stacking interaction exists between the centroids of those rings of naphthalene that are directly attached with chelating oxygens with the distance of 3.474(4) Å having zero slippage as shown in Figure 4 and given in Table 3. In addition to non-classical H-bonding and π – π stacking interaction, another weak interaction of type C–H–Cg is found that assists in further strengthening of packing of molecules in crystal structure where Cg is the centroid of one of the benzene

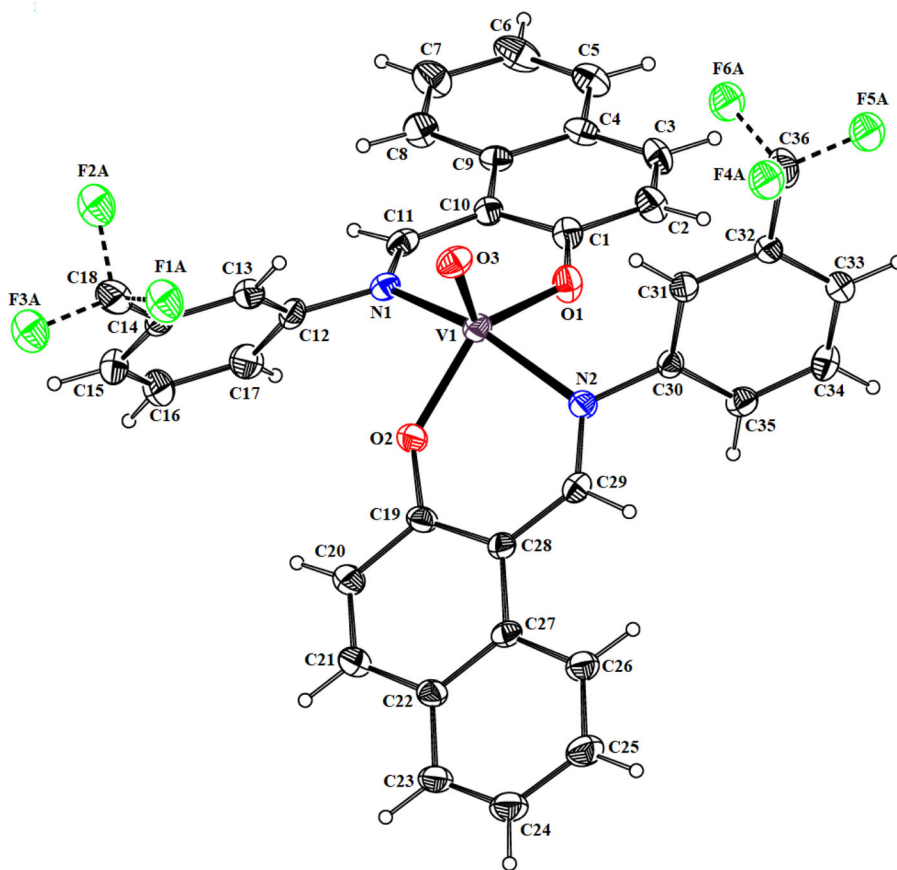


Figure 3. ORTEP diagram of **3** drawn at 20% probability level. The minor parts of disordered trifluoro moiety are not shown for clarity and the hydrogens are shown by small circles of arbitrary radii.

rings of naphthalene (C1–C10) directly attached to O-atom of (*Z*)-3-iminoprop-1-en-1-ol moiety A as given in Table 2.

In order to investigate the intermolecular interactions quantitatively, Hirshfeld surface inspection is carried out on crystal Explorer version 3.1 [43]. Figure S6 shows 2D plots for HL¹, HL⁴ and **3**. These plots give the % contribution of each interatomic contact with respect to overall interactions [44a–c]. It is found that the most significant contribution for crystal packing in HL¹, HL⁴ and **3** is from F–H/H–F interatomic contact including reciprocal contact with % contribution of 29.3%, 24.6% and 31.4%, respectively. The % contribution of F–H interatomic contact in HL⁴ is less than in HL¹ due to presence of electronegative Cl-atom in HL⁴. The % contribution of F–H interatomic contact is largest in **3** as compared to HL¹ and HL⁴ because **3** has more fluorine and H-atoms compared to HL¹ and HL⁴.

3.4. Thermogravimetric studies

Room temperature stability for **1** and **2** was revealed by its thermogravimetric analysis, carried out from ambient temperature to 1000 °C in nitrogen atmosphere. Complex **1**

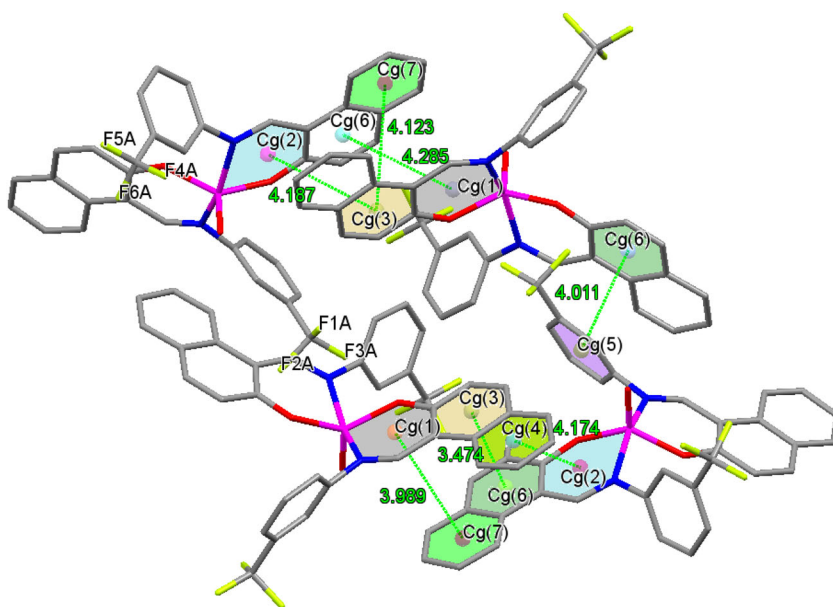


Figure 4. Graphical representation of π - π stacking interaction for **3**; only major parts of disordered trifluoro moieties are shown also H-atoms are also omitted for clarity.

showed first decomposition stage in the range of 77–447 °C. The mass loss at this temperature range may be corresponds to elimination of organic moiety, that is, $C_7H_4F_3$ (found/calc.: 24.04/24.37%). The second decomposition step from 447 to 765 °C corresponds to CF_3 (found/calc.: 11.41/11.59%). The third decomposition step occurred in the temperature range of 765–952 °C, which corresponds to the loss of another organic species, $CH-C-CH$ (found/calc.: 7.16/6.38%) leaving metal oxide and organic moiety behind, that is, $C_{17}H_{12}N_2O_3V$ (found/calc.: 57.40/57.66%).

In thermogram of **2**, the first step is elimination of CF_3 and two hydroxyl groups (2OH) in the temperature range of 24–324 °C (found/calc.: 16.30/16.41%), the second decomposition step ranged from 324 to 741 °C with the loss of two aromatic rings, C_7H_5N and $C_7H_4F_3$ (found/calc.: 39.32/39.52%), whereas the third step ranged from 741 to 951 °C with the loss of one more aromatic ring C_7H_5N and $C-CH$ (found/calc.: 19.83/20.26%) leaving metal oxide and organic moiety behind, that is, $C_4H_2O_3V$ (found/calc.: 24.39/23.81%). These observations further support the composition of **1** and **2**, which are in agreement with a result obtained by elemental studies and single-crystal analysis. Thermograms of **1** and **2** are shown in Figures S7 and S8.

3.5. Magnetic moment studies

The effective magnetic moment per metal atom was calculated from the equation:

$$\mu_{\text{eff}} = 797.5 \sqrt{\chi_m \cdot T}$$

where χ_m is the molar susceptibility of the complex which is obtained after applying diamagnetic corrections by the use of Pascal's constant for other atoms and groups in the complex. The calibrant used was $Hg[Co(SCN)_4]$. The oxidovanadium(IV) complexes

usually exhibit low magnetic moments due to the presence of only one unpaired electron in its outer shell. The magnetic moments obtained at 298 K for **1–4** under study were found to be 1.84, 2.17, 2.10 and 2.00 BM, revealing distorted square pyramidal geometry around the V(IV)O ion [45]. The values correspond to a system which has, formally, a single unpaired electron that is assumed to be localized into an orbital of primarily d-orbital character. The data demonstrate that the metal ion of these 3d¹-oxidovanadium(IV) complexes is not involved in magnetic exchange with the neighboring metal ion or atoms [46].

3.6. Electronic absorption titration

A compound can bind to DNA through intercalation, groove binding or electrostatic interactions. Intercalation usually results in hypochromism and bathochromism, due to strong π - π^* stacking interaction between an aromatic chromophore and nitrogenous base pairs of DNA. It is generally accepted that the extent of hypochromism in the UV band is related with the extent of intercalative interaction [47]. On the other hand, hyperchromism is because of electrostatic binding [31].

The UV-vis titrations of HL¹-HL⁴ and **1–4** in the absence (a) and in presence (b-i) of SS-DNA have been studied in Tris buffer medium with the wavelength range of 600–250 nm. Successive addition of DNA produces changes in electronic absorption spectrum of the complex, indicating interaction of the complex with DNA [48]. The absorption spectra are shown in Figures 5 and S9.

The determined values of absorption bands, their shifts, binding constants (K) and Gibb's free energy (ΔG) are summarized in Table 4. Negative values of ΔG showed that the interaction of the synthesized compounds with DNA is a spontaneous process.

Incremental addition of DNA lowers the intensity of absorbance, that is, hypochromic effect in all cases, except **1**. The strong absorption of these complexes in the near UV (280–360 nm) is attributed to the long-lived triplet excited state of the aromatic moiety [49]. Complexes **3** and **4** obey the same behavior (hypochromism) as displayed by their respective free ligands HL³ and HL⁴, respectively. However, **1** dramatically changes its behavior to hyperchromism in contrast to its precursor ligand HL¹ (hypochromism). Moreover, it has shown surprisingly higher value of binding affinity as reflected from its K value ($1.81 \times 10^4 \text{ M}^{-1}$). Complex **2** had shown no interaction with DNA. Hypochromism is due to contraction of DNA helix along with other conformational changes. The hypochromism and hypochromism are associated with double-helical structure of DNA. The hypochromism with minor blue shift (1–3 nm) in HL¹ and HL³ suggests an intercalative mode as well as by outside binding (groove binding); however, the dominant mode of interaction is groove binding because $\Delta\lambda \leq 8 \text{ nm}$ [50]. Groove-binders induce little or no structural rearrangement in the DNA and show binding propensity for the AT-rich DNA pockets. The AT-rich base pairs not only possess H-bond acceptors (N3 of adenine and O2 of thymine), but can also develop favorable hydrophobic interactions between the adenine C2 hydrogens and the aromatic rings present in the DNA-binding complexes [45]. Complexes **1** and **4** show hyperchromism and hypochromism, respectively, with no blue or red shift, suggesting

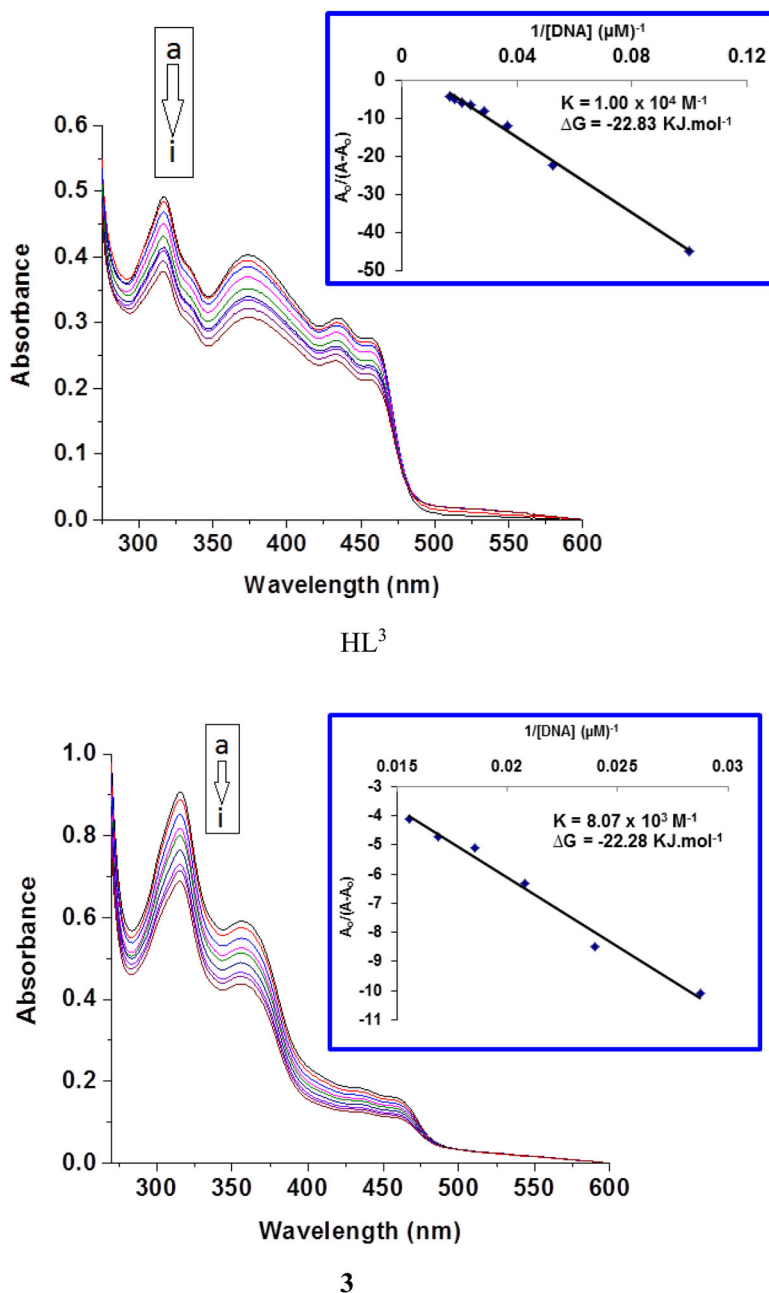
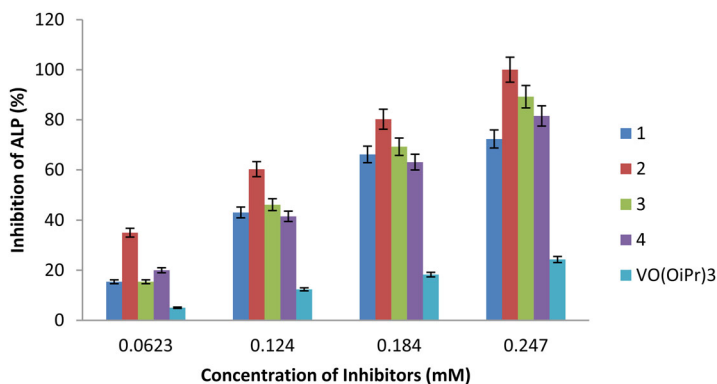


Figure 5. Absorption spectra of HL³ and 3 in the (a) absence and presence of (b) 10 μM, (c) 19 μM, (d) 27 μM, (e) 35 μM, (f) 42 μM, (g) 48 μM, (h) 54 μM and (i) 59 μM of DNA. The arrow direction indicates increasing concentrations of DNA.

intercalative mode of binding with DNA. After intercalating the base pairs of DNA the π^* orbital of the intercalated ligand could couple with π orbital of base pairs thus decreasing the $\pi-\pi^*$ transition energy. It also indicates some interaction with minor grooves which may be due to hydrogen bonding with bases [51]. On the other hand,

Table 4. Drug–DNA interaction data.

Compounds	λ_{max} (nm)	Hypochromism (%)	Hyperchromism (%)	Bathochromism (nm)	Hypsochromism (nm)	K (M^{-1}) 1×10^4	ΔG (kJ mol^{-1})
HL ¹	273	13.85	–	1	–	0.45	–20.89
1	288	–	27.3	–	–	1.81	–24.29
HL ²	308	25.34	–	–	2	0.207	–18.91
HL ³	317	23.1	–	1	–	1.00	–22.83
	374	23.5	–	3	–	–	–
3	316	24.11	–	–	1	0.80	–22.28
	356	25.88	–	–	2	–	–
HL ⁴	316	23.69	–	–	6	1.46	–23.76
4	330	28.3	–	–	–	0.17	–18.50

**Figure 6.** Concentration dependent inhibition of alkaline phosphatase (ALP) by **1–4** and VO(OiPr)₃.

the observed hypochromism with minor red shift for HL², HL⁴ and **3** revealed that drug–DNA interaction is of electrostatic interaction and groove binding type. Same results were obtained by taking the spectrum after 24 h, which confirms the stability of drug–DNA complex.

3.7. Enzyme inhibition studies

The ALP activity takes advantage of the fact that the enzyme is non-specific and utilizes the colorless non-biological substrate *p*-NPP to give yellow *p*-nitrophenolate ion upon hydrolysis which helps to monitor the reaction [52]. Free ligands HL¹–HL⁴, their respective oxidovanadium complexes **1–4** and [VO(OCHMe₂)₃] were screened for their inhibition of ALP enzyme. All ligands failed to show any activity while vanadium control the metal products (**1–4**) rendered active against ALP. The inhibition of ALPs was attributed to coordination of vanadium with enzyme to block the active sites of the enzyme. The vanadium may displace zinc or calcium from the enzyme and hence the enzyme fails to bind with the substrate. Another possibility is that the enzyme binds with the vanadium complex or vanadium ion more efficiently than substrate. The exact mechanism is still unknown [53].

The screening tests revealed that enzyme inhibition is concentration dependent. Increasing concentration of vanadium complexes decreases the activity of the enzyme as shown in Figure 6. This proportionate decrease in the activity of ALP with increase

Table 5. Antifungal activities of HL¹–HL⁴ and 1–4.

Compounds	Average zone of inhibition (mm)			
	<i>A. alternate</i>	<i>G. lucidum</i>	<i>A. niger</i>	<i>P. notatum</i>
Fluconazole	38 ^{ab} ± 0.41	41 ^{ab} ± 0.52	40 ^{ab} ± 0.36	35 ^{bc} ± 0.27
HL ¹	17 ^c ± 0.12	15 ^c ± 0.09	17 ^c ± 0.16	0
1	22 ^{bc} ± 0.15	18 ^{bc} ± 0.14	23 ^{bc} ± 0.19	21 ^c ± 0.13
HL ²	25 ^{bc} ± 0.19	21 ^{bc} ± 0.13	20 ^{bc} ± 0.08	22 ^{bc} ± 0.12
2	33 ^{ab} ± 0.26	24 ^{bc} ± 0.16	23 ^{bc} ± 0.16	35 ^{bc} ± 0.24
HL ³	30 ^{ab} ± 0.23	40 ^{ab} ± 0.30	31 ^{bc} ± 0.23	56 ^{ab} ± 0.31
3	39 ^a ± 0.28	58 ^a ± 0.33	47 ^a ± 0.29	65 ^a ± 0.36
HL ⁴	21 ^{bc} ± 0.16	19 ^{bc} ± 0.17	22 ^{bc} ± 0.15	30 ^{bc} ± 0.26
4	25 ^{bc} ± 0.17	22 ^{bc} ± 0.14	25 ^{bc} ± 0.11	27 ^{bc} ± 0.21

Concentration = 1 mg mL⁻¹ in DMSO. 0 = no activity, 5–10 = activity present, 11–25 = moderate activity, 26–40 = strong activity. Antifungal values are mean ± SD of samples analyzed individually in triplicate at $p < .1$. Different letters in superscripts indicate significant differences. a = maximum activity, b = intermediate activity, c = minimum activity, ab = activity between maximum and intermediate and bc = activity between intermediate and minimum.

Table 6. Antibacterial activities of HL¹–HL⁴ and 1–4.

Compounds	Average zone of inhibition (mm)			
	<i>E. coli</i>	<i>B. subtilis</i>	<i>S. aureus</i>	<i>P. multocida</i>
Streptomycin	30 ^{ab} ± 0.26	30 ^a ± 0.19	30 ^a ± 0.23	30 ^a ± 0.29
HL ¹	18 ^{bc} ± 0.11	19 ^{bc} ± 0.17	18 ^{bc} ± 0.13	18 ^{bc} ± 0.16
1	25 ^{ab} ± 0.19	22 ^{bc} ± 0.13	24 ^b ± 0.16	25 ^{ab} ± 0.22
HL ²	17 ^c ± 0.14	20 ^{bc} ± 0.16	19 ^{bc} ± 0.17	20 ^{bc} ± 0.14
2	30 ^{ab} ± 0.21	21 ^{bc} ± 0.13	25 ^{ab} ± 0.20	24 ^{ab} ± 0.19
HL ³	17 ^c ± 0.12	17 ^c ± 0.10	17 ^c ± 0.15	16 ^c ± 0.11
3	31 ^a ± 0.23	25 ^{ab} ± 0.18	22 ^{bc} ± 0.19	29 ^{ab} ± 0.27
HL ⁴	26 ^{ab} ± 0.19	17 ^c ± 0.11	24 ^b ± 0.15	21 ^{bc} ± 0.18
4	28 ^{ab} ± 0.19	23 ^{bc} ± 0.15	26 ^{ab} ± 0.17	26 ^{ab} ± 0.16

Concentration = 1 mg mL⁻¹ in DMSO. 0 = no activity, 5–10 = activity present, 11–25 = moderate activity, 26–40 = strong activity. Antibacterial values are mean ± SD of samples analyzed individually in triplicate at $p < .1$. Different letters in superscripts indicate significant differences. a = maximum activity, b = intermediate activity, c = minimum activity, ab = activity between maximum and intermediate and bc = activity between intermediate and minimum.

in the concentration of complexes indicates anti-enzymatic activity. Complex **2** was observed as the most potent inhibitor against all the concentrations of ALP studied. This could probably be due to the presence of an extra free (–OH') which may result in the development of stronger enzyme–complex interactions and consequent failure of the ALP to bind with the target substrate. Hence, there is a less amount of product formation resulting in a decrease in absorption.

3.8. Antimicrobial activities

The synthesized free ligands and their respective vanadium products were screened for their *in vitro* response against various strains of fungi (*A. alternata*, *G. lucidum*, *A. niger* and *P. notatum*) and bacteria (*E. coli*, *B. subtilis*, *S. aureus* and *P. multocida*) by a modified [33] disc diffusion method [34]. Fluconazole and Streptomycin were used as the positive controls for antifungal and antibacterial screening tests, respectively, while DMSO was used as a negative control. The data are summarized in Tables 5 and 6. The vanadium complexes exhibited significantly higher activities towards the tested

Table 7. Hemolytic activities of HL¹–HL⁴ and **1**–**4**.

Compound	% of hemolysis
HL ¹	77.77 ± 0.03
1	58.46 ± 0.04
HL ²	32.40 ± 0.02
2	52.26 ± 0.03
HL ³	32.79 ± 0.03
3	42.21 ± 0.02
HL ⁴	34.65 ± 0.03
4	44.39 ± 0.01
Triton-X 100	99.53 ± 0.72

organisms than their respective free azomethine precursors, which indicate that metalation has increased the antimicrobial potential in accord with earlier reports [54]. This increased activity may be attributed to the chelation of the metal with the ligand as the chelation reduces the polarity of the central metal atom because of partial sharing of its positive charge with the ligand, which favors the permeation of the complex through the lipid layer of the membrane [55].

There is a close relationship between structure and antimicrobial activities of the investigated products [56]. Although the antimicrobial activities were appreciably enhanced after metal coordination in all cases against both the bacterial and fungal strains, the results observed for HL³ and its respective complex **3** were quite fascinating. The highest activity among all the ligands was observed for HL³ against all the fungal species; its corresponding complex was also found to possess the highest antifungal action than all the tested novel complexes. The activity was found even higher than the standard control drug Fluconazole. The variations in antimicrobial potencies of these compounds may be explained based on two possible factors, that is, lipophilic character and diffusion on the bacterial strain [57]. So the highest antifungal activity of HL³ and **3** was rendered to their more bulky structures which resulted in greater lipophilicity and hence their greater diffusion through the microbial cell membrane, thus ultimately causing greater sensitivity of the microbes towards these two drugs. The difference in the effectiveness of various biocidal agents against different organisms depends upon the permeability through cell membranes [58].

3.9. Hemolytic activities

Hemolytic activity was studied because, even if a synthesized compound possesses potent antimicrobial activities, its use in medicine will be impossible without their hemolytic investigations. The *in vitro* hemolytic bioassays of the synthesized complexes were performed with human red blood cells and the average lysis was reported with respect to the Triton X-100 as positive control (100% lysis) and PBS as negative control (0% lysis). The results obtained are summarized in Table 7. The data revealed that all the synthesized complexes possessed significantly lower hemolytic activities as compared to Triton X-100 and higher than PBS. The cytotoxicity was found to increase in the investigated complexes **2**–**4** in relation to the respective ligands HL²–HL⁴, however it was decreased in the case of vanadated product **1** as compared to the non-coordinated free ligand, HL¹. Therefore, the compounds showing the highest activity may be considered for the antitumor activity [59].

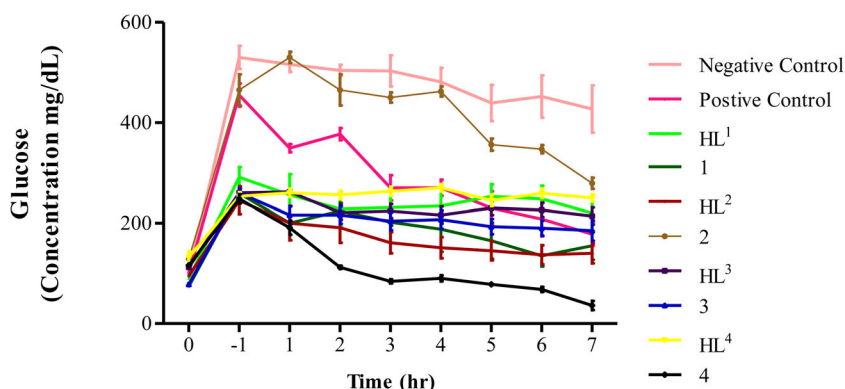


Figure 7. Plasma glucose concentration of mice treated with the synthesized compounds. Negative control was Alloxan only treated, while positive control was treated with Glibenclamide. $**p < .001$.

3.10. Antidiabetic studies

Antidiabetic potential of oxidovanadium complexes and their respective precursors were tested on BALB/c albino mice [60]. In general, the animals remained healthy and active. Deaths occurred in HL¹ and **3**. For obvious reasons, compounds that showed glucose lowering, their results were compared with Glibenclamide, while compounds that led to an increase in plasma glucose, cholesterol and triglycerides, their results were compared with only Alloxan treated negative control mice. The results are presented in Figures 7 and 8.

HL¹ did not show any glucose lowering activity (Figure 7), it raised triglyceride concentration significantly ($p < .001$; Figure 8(A)) and reduced cholesterol concentration ($p < .001$; Figure 8(B)). Injection of **1** led to a significant lowering of plasma glucose ($p < .001$; Figure 7), triglyceride ($p < .003$; Figure 8(A)) and cholesterol concentrations ($p < .002$; Figure 8(B)).

HL² significantly reduced plasma glucose ($p < .001$; Figure 7) and serum cholesterol concentrations ($q = 3.693$; Figure 8(B)) but increased the serum triglyceride concentration ($p < .002$; Figure 8(A)). Complex **2** did not cause any significant change in plasma glucose (Figure 7) and serum cholesterol (Figure 8(B)) concentrations, but increased in serum triglyceride concentration significantly (Figure 8(A)).

No significant change was caused by HL³ in plasma glucose (Figure 7) or cholesterol (Figure 8(B)) concentrations but caused significant elevation of serum triglyceride concentration (Figure 8(A)). Similarly, no significant change was caused by **3** in either glucose or cholesterol concentrations (Figures 7 and 8(B)) but caused significant increase in triglyceride concentration (Figure 8(A)).

HL⁴ significantly lowered plasma glucose ($p < .002$; Figure 7) and serum cholesterol concentrations ($q = 3.693$; Figure 8(B)) but no variation was observed in triglyceride concentration (Figure 8(A)). Complex **4** led to a significant reduction in plasma glucose, serum cholesterol and triglyceride concentrations ($p < .001$; Figures 7 and 8(B) and (A)).

The present study revealed that **1** and **4** possess exactly similar activity as they lowered the serum glucose, cholesterol and triglyceride concentrations simultaneously. **2**, HL³ and **3** appear to be exactly similar in their activity as they showed significant elevation of serum triglyceride concentration but caused no change in glucose and cholesterol concentration.

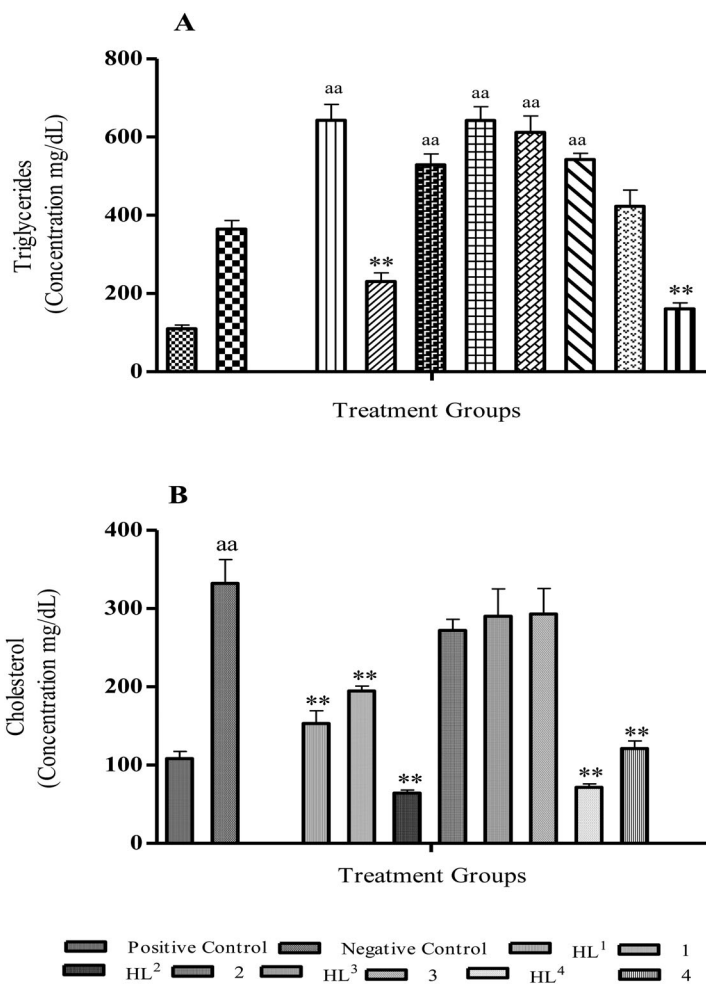


Figure 8. Serum triglyceride and cholesterol concentrations of mice treated with oxidovanadium complexes and azomethine precursors. Results were compared against Alloxan and Glibenclamide treated animals. ** $p < .001$ (showing significant increase); ^{aa} $p < .001$ (showing significant decrease).

1 and HL⁴ appeared to be similar in lowering glucose and cholesterol concentrations but showed different behavior for triglyceride concentration. Complex **1** decreased triglyceride whereas HL⁴ did not cause any change. Lastly, HL¹ appeared to be totally different in its activity as it did not cause any change in glucose concentration, however, caused a decrease in cholesterol concentration and raised the triglyceride concentration but, on the other hand, **1** has significant activity in all respects.

Among all the eight compounds tested, HL¹ and **3** have proved to be relatively highly toxic as their application led to mortalities of animals.

4. Conclusion

A series of new azomethine precursors and their oxidovanadium(IV) complexes were synthesized and characterized by elemental analysis, FT-IR and NMR spectroscopies,

thermogravimetry, magnetic moment and X-ray crystallography. FT-IR and single-crystal X-ray crystallography studies revealed that during complexation of ligands with metal ion, the binding occurred through azomethine nitrogen and phenolic oxygen of the precursors. Therefore, the ligands behaved as monobasic, bidentate during formation of complexes. The paramagnetic properties of the vanadium complexes **1–4** confirmed the d^1 electronic configuration of vanadium. The mode of binding of the compounds and their complexes with SS-DNA was investigated by UV–Visible spectroscopy. The observed hypochromicity indicated the intercalation mode of binding of compounds with SS-DNA. The improved biological activities of the azomethine linkage or heteroaromatic nuclei during complexation may be responsible for the increase in hydrophobic character and liposolubility of the molecules in crossing the cell membrane of the microorganism and enhance biological utilization ratio and activity of complexes.

Disclosure statement

No potential conflict of interest was reported by the authors.

Funding

Higher Education Commission under Indigenous This work was supported by the Higher Education Commission under Indigenous 5000 Program [PIN NO. 106-1087-ps6-016].

References

- [1] A. Kumar, A. Dixit, S. Sahoo, S. Banerjee, A. Bhattacharyya, A. Garai, A.A. Karande, A.R. Chakravarty. *J. Inorg. Biochem.*, 202, 110817 (2020).
- [2] D. Althumairy, H.A. Murakami, D. Zhang, B.G. Barisas, D.A. Roess, D.C. Crans. *J. Inorg. Biochem.*, 203, 110873 (2020).
- [3] V.H. Rambaran, S.M. Saumya, S. Roy, K.P. Sonu, M. Eswaramoorthy, S.C. Peter. *Inorg. Chim. Acta*, 504, 119448 (2020).
- [4] A. Hasnaoui, I. Hdoufane, A. Alahyane, A. Nayad, D. Cherqaoui, M.A. Ali, L. El Firdoussi. *Inorg. Chim. Acta*, 501, 119276 (2020).
- [5] I. El-Deen, A. Shoair, M. El-Bindary. *J. Mol. Struct.*, 1180, 420 (2019).
- [6] A.D. Giuseppe, C.D. Nicola, R. Pettinari, I. Ferino, D. Meloni, M. Passacantando, M. Crucianelli. *Catal. Sci. Technol.*, 3, 1972 (2013).
- [7] C. Kavitha, P. Subramaniam. *Polyhedron*, 175, 114172 (2020).
- [8] M. Abdi, A.F. Shojaei, M. Ghadermazi. *Acta Chim. Sloven*, 67, 1 (2020).
- [9] M.W. Makinen, M. Salehitazangi. *Coord. Chem. Rev.*, 279, 1 (2014).
- [10] N. Domingues, J. Pelletier, C.G. Ostenson, M.M. Castro. *J. Inorg. Biochem.*, 131, 115 (2014).
- [11] L. Zhao, H-y Wei, M-j Lv. *Guangzhou Chem. Ind.*, 12, 87 (2013).
- [12] Y.-L. Sang, X.-H. Zhang, X.-S. Lin, Y.-H. Liu, X.-Y. Liu. *J. Coord. Chem.*, 73, 164(2020).
- [13] P. Ying, X. Tian, P. Zeng. *Med. Chem.*, 4, 549 (2014).
- [14] E.A. Enyedy, G.M. Bognar, N.V. Nagy, T. Jakusch, T. Kiss, D. Gambino. *Polyhedron*, 67, 242 (2014).
- [15] A.A. Holder, P. Taylor, A.R. Magnusen, E.T. Moffett, K. Meyer, Y. Hong, S.E. Ramsdale, M. Gordon, J. Stubbs, L.A. Seymour, D. Acharya, R.T. Weber, P.F. Smith, G.C. Dismukes, P. Ji, L. Menocal, F. Bai, J.L. Williams, D.M. Cropek, W.L. Jarrett. *Dalton Trans.*, 42, 11881 (2013).

- [16] M.A. Neelakantan, F. Rusalraj, J. Dharmaraja, S. Johnsonraja, T. Jeyakumar, M.S. Pillai. *Spectrochim. Acta A Mol. Biomol. Spectrosc.*, 71, 1599 (2008).
- [17] Y.-J. Liu, X.-Y. Guan, X.-Y. Wei, L.-X. He, W.-J. Mei, J.-H. Yao. *Transit. Met. Chem.*, 33, 289 (2008).
- [18] L. Jia, P. Jiang, J. Xu, Z. Hao, X. Xu, L. Chen, J. Wu, N. Tang, Q. Wang, J.J. Vittal. *Inorg. Chim. Acta*, 363, 855 (2010).
- [19] U. Saha, K.K. Mukherjea. *Int. J. Biol. Macromol.*, 66, 166 (2014).
- [20] J.Z. Lu, Y.F. Du, H.W. Guo, J. Jiang, X.D. Zeng, L.Q. Zang. *J. Coord. Chem.*, 64, 1229 (2011).
- [21] P.K. Sasmal, S. Saha, R. Majumdar, R.R. Dighe, A.R. Chakravarty. *Inorg. Chem.*, 49, 849 (2010).
- [22] X.W. Li, Y. Yu, Y.T. Li, Z.Y. Wu, C.W. Yan. *Inorg. Chim. Acta*, 367, 64 (2011).
- [23] K. Hiwada, E.D. Wachsmuth. *Biochem. J.*, 141, 293 (1974).
- [24] S. Shirazi, R. Beechey, P. Butterworth. *Biochem. J.*, 194, 803 (1981).
- [25] D.C. Crans, J.J. Smees, E. Gaidamauskas, L. Yang. *Chem. Rev.*, 104, 849 (2004).
- [26] R. Chander, P. Thomas. *J. Food Biochem.*, 25, 91 (2001).
- [27] R.L. Dean. *Biochem. Mol. Biol. Educ.*, 30, 401 (2002).
- [28] M. Ashfaq, M.N. Tahir, A. Kuznetsov, S.H. Mirza, M. Khalid, A. Ali. *J. Mol. Struct.*, 1199, 127041 (2020).
- [29] S. Dey, S. Sarkar, H. Paul, E. Zangrando, P. Chattopadhyay. *Polyhedron*, 29, 1583 (2010).
- [30] C.V. Sastri, D. Eswaramoorthy, L. Giribabu, B.G. Maiya. *J. Inorg. Biochem.*, 94, 138 (2003).
- [31] S. Shujha, A. Shah, N. Muhammad, S. Ali, R. Qureshi, N. Khalid, A. Meetsma. *Eur. J. Med. Chem.*, 45, 2902 (2010).
- [32] M.R. Malik, V. Vasylyeva, K. Merz, N.M. Nolte, M. Saleem, S. Ali, A.A. Isab, K.S. Munawar, S. Ahmad. *Inorg. Chim. Acta*, 376, 207 (2011).
- [33] S. Hussain, S. Ali, S. Shahzadi, M.N. Tahir, M. Shahid. *J. Coord. Chem.*, 68, 2369 (2015).
- [34] CLSI (the Clinical Laboratory Standards Institute). *J. Clin. Microbiol.*, 45, 2758 (2007).
- [35] S. Hussain, S. Ali, S. Shahzadi, M. Shahid. *Cogent. Chem.*, 1, 1029038 (2015).
- [36] W.A. Powell, C.M. Catranis, C.A. Maynard. *Lett. Appl. Microbiol.*, 31, 163 (2000).
- [37] C.R. Bhattacharjee, C. Datta, G. Das, P. Mondal. *Phase Trans.*, 85, 956 (2012).
- [38] S. Bhattacharyya, S. Mukhopadhyay, S. Samanta, T.J.R. Weakley, M. Chaudhury. *Inorg. Chem.*, 41, 2433 (2002).
- [39] M. Hussain, M. Hanif, S. Ali, M. Altaf, H.S. Evans. *Acta Cryst.*, E62, 5020 (2006).
- [40] J. Bernstein, R.E. Davis, L. Shimon, N.-L. Chang. *Angew. Chem. Int. Ed. Engl.*, 34, 1555 (1995).
- [41] A.W. Addison, T.N. Rao, J. Reedijk, J. van Rijn, G.C. Verschoor. *J. Chem. Soc. Dalton Trans.*, 1349 (1984).
- [42] S.K. Seth. *Acta Crystallogr. E Crystallogr. Commun.*, 74, 600 (2018).
- [43] S.K. Wolff, D.J. Grimwood, J.J. McKinnon, M.J. Turner, D. Jayatilaka, M.A. Spackman. *Crystal Explorer (Version 3.0)*, University of Western Australia, Perth, Australia (2012).
- [44] (a) A.S. Mark, J. Dylan. *CrystEngComm*, 11, 19 (2009);(b) J. Zukerman-Schpector, S.D. Pedroso, L.S. Madureira, M.W. Paixão, A. Ali, E.R.T. Tiekink. *Acta Cryst.*, E73, 1716 (2017);(c) A. Ali, J. Zukerman-Schpector, M.W. Paixão, M.M. Jotani, E.R.T. Tiekink. *Acta Cryst.*, E74, 184 (2018).
- [45] R. Maurya, S. Rajput. *J. Mol. Struct.*, 687, 35 (2004).
- [46] Y. Zhang, X. Wang, W. Fang, X. Cai, F. Chu, X. Liao, J. Lu. *Bioinorg. Chem. Appl.*, 2013, 437134 (2013).
- [47] A.G. Cherstvy. *Phys. Chem. Chem. Phys.*, 13, 9942 (2011).
- [48] S.T. Hafeez, M.N. Tahir, S. Ali, M. Iqbal, H. Gulab, K.S. Munawar. *J. Coord. Chem.*, 68, 3636 (2015).
- [49] M. Sirajuddin, S. Ali, A. Haider, N.A. Shah, A. Shah, M.R. Khan. *Polyhedron*, 40, 19 (2012).
- [50] S.S. Kalanur, U. Katrahalli, J. Seetharamappa. *J. Electroanal. Chem.*, 636, 93 (2009).
- [51] J.B. Chaires. *Arch. Biochem. Biophys.*, 453, 26 (2006).
- [52] F. Javed, S. Ali, M.W. Shah, K.S. Munawar, S. Shahzadi, Hameedullah, H. Fatima, M. Ahmed, S.K. Sharma, K. Qanungo. *J. Coord. Chem.*, 67, 2795 (2014).

- [53] K.S. Munawar, S. Ali, M.N. Tahir, N. Khalid, Q. Abbas, I.Z. Qureshi, S. Shahzadi. *Russ. J. Gen. Chem.*, 85, 2183 (2015).
- [54] E.R.T. Tiekink. *Appl. Organometal. Chem.*, 22, 533 (2008).
- [55] M. Carcelli, A. Fochi, P. Pelagatti, G. Pelizzi, U.J. Russo. *J. Organomet. Chem.*, 626, 161 (2001).
- [56] S. Hussain, S. Ali, S. Shahzadi, C. Rizzoli, M. Shahid. *J. Chin. Chem. Soc.*, 62, 793 (2015).
- [57] B. Parveen, I.H. Bukhari, S. Shahzadi, S. Ali, S. Hussain, K.G. Ali, M. Shahid. *J. Serb. Chem. Soc.*, 80, 755 (2015).
- [58] T.M. Fyles. *Chem. Soc. Rev.*, 36, 335 (2007).
- [59] A. Rehman, S.Z. Siddiqui, M.A. Abbasi, N. Abbas, K.M. Khan, M. Shahid, Y. Mahmood, M.N. Akhtar, N.H. Lajis. *Int. J. Pharm. Pharm. Sci.*, 676, 4 (2012).
- [60] Z. Iqbal, S. Ali, S.J. Iqbal, Q. Abbas, I.Z. Qureshi, S. Hameed. *Bioorg. Med. Chem. Lett.*, 23, 488 (2013).